J Mol Model (2013) 19:3201–3217
DOI 10.1007/s00894-013-1820-1

ORIGINAL PAPER

Synthesis and biological evaluation of cationic fullerene quinazolinone conjugates and their binding mode with modeled *Mycobacterium tuberculosis* hypoxanthine-guanine phosphoribosyltransferase enzyme

Manishkumar B. Patel · Sivakumar Prasanth Kumar · Nikunj N. Valand · Yogesh T. Jasrai · Shobhana K. Menon

Received: 2 February 2013 / Accepted: 7 March 2013 / Published online: 30 April 2013

Abstract The present work reports a series of novel cationic fullerene derivatives bearing a substituted-quinazolinone moiety as a side arm. Fullerene-quinazolinone conjugates synthesized using the 1,3-dipolar cycloaddition reaction of C_{60} with azomethine ylides generated from the corresponding Schiff bases of substituted quinazolinone were characterized by elemental analysis, FT-IR, ^{1}H NMR, ^{13}C NMR and ESI-MS and screened for their antibacterial activity against *Mycobacterium tuberculosis* (*$H_{37}Rv$* strain). All the compounds exhibited significant activity with the most effective having MIC in the range of 1.562–3.125 μg/mL. Compound 9f exhibited good biological activity compared to standard drugs. We developed a computational strategy based on the modeled *M. tuberculosis* hypoxanthine-guanine phosphoribosyltransferase (HGPRT) using homology modeling techniques and studied its binding pattern with synthesized fullerene derivatives. We then explored the surface geometry of the protein to place the cage adjacent to the active site while optimizing its quinazolinone side arm to establish H bonding with active site residues.

Keywords Fullerene · Antimycobacterial activity · Homology modeling

Abbreviations

AMBER	Assisted model building with energy refinement
BCG	Bacillus Calmette-Guérin
BLAST	Basic local alignment search tool
CSP	Constraint space programming
E value	Expected value
EC	Enzyme classification
ExPASy	Expert protein analysis system
GA	Genetic algorithm
GB	Generalized born
HGPRT	Hypoxanthine-guanine phosphoribosyltransferase
MDR-TB	Multi drug resistance tuberculosis
PB	Poisson-boltzmann
PEARLS	Program of energetic analysis of receptor ligand systems
PP_i	Inorganic pyrophosphate
PRPP	α-D-phosphoribosyl-1-pyrophosphate
PRPP	Phosphoribosyl pyrophosphate
PRT	Phosphoribosyl transferase
QMEAN	Qualitative model energy analysis
RCSB PDB	Research collaborative for structural bioinformatics protein data bank
SAVES	Structural analysis and verification server
SCRs	Structurally conserved regions
TB	Tuberculosis
TMS	Tetra methyl silane

M. B. Patel · N. N. Valand · S. K. Menon (✉)
Department of Chemistry, University School of Sciences, Gujarat University, Ahmedabad, Gujarat 380009, India
e-mail: shobhanamenon07@gmail.com

S. P. Kumar · Y. T. Jasrai
Department of Bioinformatics, Applied Botany Centre (ABC), University School of Sciences, Ahmedabad, Gujarat 380009, India

Introduction

The World Health Organization (WHO) recognizes tuberculosis (TB)—a disease of poverty—as one of the prime causes of mortality worldwide, with an estimated global rate of TB infection of 8.8 million including 1.1 million HIV-

infected cases in 2010 [1]. The current scenario is worsened further by the prevalence of multi drug resistant TB (MDR-TB) infection, HIV co-infection, lack of patient compliance with chemotherapy and inconsistent efficacy of the BCG vaccine [2]. Thanks to a recent initiative by WHO to introduce new diagnostic measures in 145 developing countries, there are renewed hopes of reducing the mortality rate of asymptomatic TB, but the lengthy chemotherapy (6–9 months) required essentially paves way for multi drug resistance by the bacterium, in addition to the drug's significant toxicity [3, 4]. There is an urgent need to identify more potent and selective antituberculosis drugs that inhibit essential biosynthetic and salvage pathways besides the conventional drug targets for which the bacterium have already developed resistance mechanisms [5].

The emergence of fullerene was marked by bulk production in the year 1990. To date, fullerene has demonstrated a wide spectrum of applications in the biological and medicinal chemistry arena. Fullerene and its scaffold exhibit various activities and uses, including antibacterial [6], antimycobacterial [7], neuroprotective [8], antioxidant [9, 10],DNA cleavage [11, 12], HIV protease inhibitors [13, 14], potentiometric biosensing of glucose [15], gene carrier [16], drug delivery systems [17], etc. Fullerene has opened up a new window in diagnosis and therapeutics due to its promising role in crossing cell membranes; this role has been attributed to its lipophilic carbon cage [18].

The quinazolin-4(3H)-one side arm has been studied due to the versatility of the quinazolinone scaffold. Quinazolinone derivatives are readily accessible, have diverse chemical reactivity and a wide range of biological activities (antibacterial [19], anti-inflammatory [20], antioxidant [21], and antimycobacterial [22–24]). Quinazolinone has been shown to inhibit important *M. tuberculosis* enzymes including purine nucleoside phosphorylase [25], enoyl-[acyl-carrier-protein] reductase (InhA), purine nucleoside phosphorylase (PNP), shikimate kinase [26], etc. The quinazoline moiety was also considered as a functional chemical unit for extensive structure-based drug design using molecular docking techniques [27] and molecular dynamic (MD) simulations [28, 29]. Cationic fullerene nanoparticles, despite being capable of crossing the cell wall, influence the inhibition of microbial growth in cell culture and play an indirect role in energy metabolism perturbations conferred by the side arm. Further, quinazolinone and analogous heterocyclic compounds play a role as enzymatic inhibitors pertaining to bacterium central metabolism [30]. It should also be noted that quinazolinone compounds are potent inhibitors of hypoxanthine-guanine phosphoribosyltransferase (HGPRT; EC 2.4.2.8)—an essential enzyme in the salvage pathway of central metabolism [31]. Recently, using a reverse docking approach, HGPRT was found to be the most favorable protein target of fullerenes [32].

In the present paper, we propose the synthesis of cationic fullerene-quinazolinone conjugates with substituted quinazolinone having a Schiff base group as a linker, which provides a synergistic enhancement of antimycobacterial activities. Furthermore, it is known that substitutions at the 2nd, 3rd, 6th and 8th positions of the quinazolinone ring gives improved antimycobacterial activity. A bioinformatic study was carried out to model *M. tuberculosis* HGPRT using homology modeling procedures, and its structural features were investigated to understand ligand binding conformity. Subsequently, molecular docking of fullerene derivatives was performed to identify potential interaction patterns with active residues and elucidate the binding mode.

Materials and methods

Experimental procedures

All chemicals and reagents were of analytical grade and purchased from BDH (https://us.vwr.com), Aldrich (St. Louis, MO) and Merck (Darmstadt, Germany) unless otherwise specified. The solvents used for analysis were purified by standard methods [49]. Melting points (°C, uncorrected) were taken using an MPA100 Automated Melting Point Apparatus. FT-IR spectra were recorded on a Bruker Tensor 27 FT-IR spectrometer with KBr pellets. ESI-MS spectra were recorded on an API 2000 LC/MS/MS System (Applied Biosystems, Foster City, CA). The elemental analysis system used was a Vario Micro cube elementar analyzer (http://www.elementar.de/en/products/elementar-products/vario-micro-cube/), and ^{1}H NMR and ^{13}C NMR spectra were recorded on a Bruker Avance II 400 MHz spectrometer in DMSO or $CDCl_3$ with tetra methyl silane (TMS) as an internal standard. The progress of the reaction was monitored on ready-made silica gel plates (Merck) using toluene: ethyl acetate as the solvent system. Spectral data (FT-IR, ^{1}HNMR, mass spectra and elemental analysis) confirmed the structure of the synthesized compounds, and purity was ascertained by microanalysis. Elemental (C, H, N) analysis indicated that the calculated and observed values were within acceptable limits (±0.4 %).

The route adopted for the synthesis of fullerene quinazolinone conjugates is as shown in Figs 1 and 2. The synthetic intermediates—substituted-2-methyl-benzoxazin-4(3H)-ones (**3a–c**)—were obtained in high yield when a mixture of unsubstituted/substituted anthranilic acid **2a–c** and acetic anhydride were refluxed under anhydrous conditions for 4 h. Similarly, substituted-2-phenyl-benzoxazin-4(3H)-ones (**3d–f**) were obtained by reacting unsubstituted/substituted anthranilic

acid **2a–c** with benzoyl chloride using pyridine as the hydrochloride scavenger.

The substituted-benzoxazin-4[3H]-ones (**3a–f**) were then converted to substituted-4- ethyl-4-[oxo(3H)quinazoline-3-yl)-benzoate (**4a–f**) by fusion with ethyl-*p*-aminobenzoate at 140 °C, which, with excess hydrazine hydrate, afforded the corresponding 4-(substituted -4-oxo-(3H)-quinazoline-3-yl)-benzoic acid hydrazide (**5a–f**) (Fig. 1). Schiff bases (**6a–f**) were formed by treating (**5a–f**) with mono protected teraphthaldehyde in ethanol and glacial acetic acid. Deprotection of the aldehyde group was then achieved by treating with perchloric acid using dioxane as solvent to obtain 4-(substituted-4-oxo-(3H)-quinazoline-3-yl)-4-formyl-benzylidene hydrazide (**7a–f**) (Fig. 2).

Compounds (**7a–f**), N-methyl glycine and (C_{60}) fullerene were then allowed to reflux in toluene, wherein they undergo a 1,3 dipolar cycloaddition reaction [50] to give fulleropyrrolidines (**8a–f**) (Fig. 2). The cationic derivatives (**9a–f**) (Fig. 2) were obtained by refluxing (**8a–f**) with methyl iodide in chloroform for 2 days.

Synthesis of unsubstituted/substituted benzoxazin-4(3H)-ones (3a–f) was carried out as reported earlier [51, 52]. The synthesis of ethyl 4-(substituted-4-oxo-(3H) quinazolin-3-yl) benzoate (**4a–f**) and 4-(substituted-4-oxo-(3H) quinazolin-3-yl)-benzoic acidhydrazide (**5a–f**) was carried out using reported methods [34]. The synthesized compounds were characterized by elemental analysis, FT-IR, ^{1}H NMR, ^{13}C NMR and ESI-MS and compared with reported values.

*4-[substituted-4-oxo-(3H) quinazolin-3-yl]–benzoic acid (4-[1, 3] dioxolan-2yl-benzylidene)hydrazide (**6a–f**)*

The synthesis of 4-[substituted-4-oxo-(3H) quinazolin-3-yl]–benzoic acid (4-[1, 3] dioxolan-2yl-benzylidene)hydrazide (**6a–f**) was carried out following a method similar to that reported earlier [7]. A mixture of 1.79 g (0.01 mol^{-1}) 4-(1,3)-dioxolan-2yl-benzaldehyde, 2 mL glacial acetic acid, 2.941 (0.01 mol^{-1}) substituted quinazolinone **5a** dissolved in 50 mL ethanol was refluxed for about half an hour.

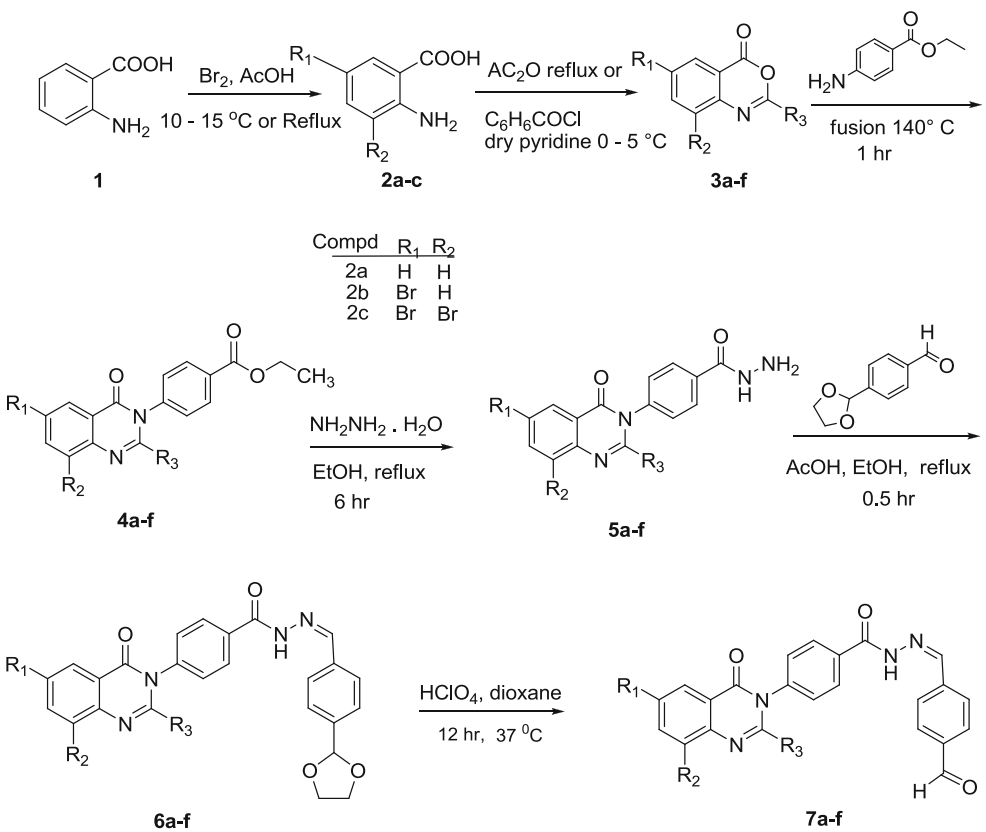

a) R_1 = H, R_2 = H, R_3 = CH_3 d) R_1 = H, R_2 = H, R_3 = C_6H_5

b) R_1 = Br, R_2 = H, R_3 = CH_3 e) R_1 = Br, R_2 = H, R_3 = C_6H_5

c) R_1 = Br, R_2 = Br, R_3 = CH_3 f) R_1 = Br, R_2 = Br, R_3 = C_6H_5

Fig. 1 Synthesis of Schiff base of substituted quinazolinone

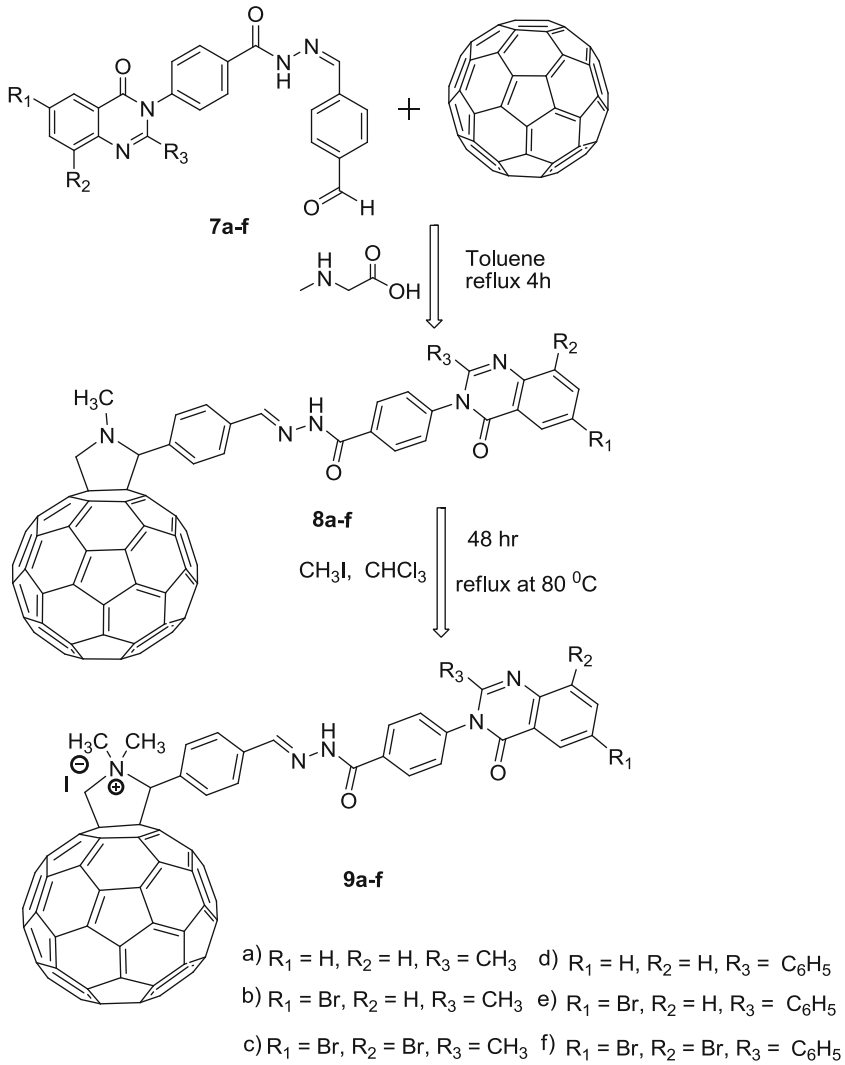

Fig. 2 Synthesis of cationic derivatives of fullerene-quinazolinone conjugates

The product was isolated and purified by column chromatography using hexane:ethyl acetate (9:1) as the eluant. The solvent was then distilled under vacuum to yield a bright yellow product (**6a**). Compounds **(6b–f)** were synthesized in an analogous manner and were characterized as shown below.

*4-(2-methyl-4-oxo-(3H) quinazolin-3-yl)–benzoic acid (4-[1, 3] dioxolan-2yl benzylidene) hydrazide (**6a**)*

Yield: 84 %, mp >240 °C; IR (KBr, υ cm^{-1}): 1659 (-C = O cyclic tertiary amide), 1680, 1535 (-C = O Acyclic secondary amide), 3300, 3190 (-NH-), 1640 (CH = N); ^{1}H NMR (δ, 400 MHz, DMSO-d_6, Me_4Si) 2.45 (s, 3H, CH_3), 5.82 (s, 1H, O-CH-O), 3.95–4.05 (m, 4H, -OCH_2-CH_2O-); 7.41–8.23 (m, 13H, Aromatic H & -N = CH), 9.98 (s, 1H, -NH); ^{13}C NMR (δ, 125 MHz, DMSO-d_6, Me_4Si) 23.33 (-CH_3), 67.47 (OCH_2-CH_2-O), 105.49 (O-CH-O), 121.90, 121.96, 125.06, 126.35, 126.74, 126.81, 127.27, 129.56, 130.23, 130.33, 133.68, 139.44, 142.67, 147.74 (Ar C) 148.27 (-N = CH), 154.04(-C = N), 161.47 (-C = O-N=), 163.93 (-C = O-NH); MS: m/z 454.50 (M+). Analysis for $C_{26}H_{22}N_4O_4$, (454.48) Calcd: % C 68.71; H 4.88; N, 12.33. Found: % C 68.72; H 4.90; N 12.34.

*4-(6-bromo-2-methyl-4-oxo-(3H) quinazolin-3-yl)-benzoic acid (4-[1, 3]dioxolan-2-ylbenzyliden) hydrazide (**6b**)*

Yield: 80 %, mp >240 °C; IR (KBr, υ cm^{-1}): 1658 (-C = O cyclic tertiary amide), 1682, 1530 (-C = O Acyclic secondary amide), 3429, 3230 (-NH-), 1668 (CH = N); ^{1}H NMR (δ, 400 MHz, DMSO-d_6, Me_4Si) 2.48 (s, 3H, CH_3), 5.89 (s, 1H, O-CH-O), 3.95–4.12 (m, 4H, -OCH_2-CH_2O-); 7.44–8.36 (m, 12H, Aromatic H & -N = CH), 10.05 (1H, s, -NH); ^{13}C NMR (δ, 125 MHz, DMSO-d_6, Me_4Si) 23.34 (-CH_3), 67.41 (OCH_2-CH_2O-), 105.23 (O-CH-O), 121.92, 126.72, 127.27, 127.34, 127.37, 128.26, 130.23, 130.21, 133.36, 133.71, 139.51, 142.62, 146.78 (Ar C) 148.22 (-N = CH), 154.12 (-C = N), 161.32 (-C = O-N=), 163.88; (-C = O-NH); MS: m/z 533.32, 535.34 (M+), (M + 2). Analysis

for $C_{26}H_{21}N_4O_4Br$ (533.37) Calcd: % C 58.55; H 3.97; N 10.50. Found: % C 58.56; H 3.98; N 10.52.

*4-(6,8-dibromo-2-methyl-4-oxo-(3H)quinazolin-3-yl)-benzoic acid (4-[1, 3]dioxolan-2-ylbenzyliden) hydrazide (**6c**)*

Yield: 79 %, mp >240 °C; IR (KBr, υ cm^{-1}): 1651 (-C = O cyclic tertiary amide), 1675, 1529 (-C = O Acyclic secondary amide), 3323, 3187(-NH-), 1635 (CH = N); ^{1}H NMR (δ, 400 MHz, DMSO-d_6, Me_4Si) 2.39 (s, 3H, CH_3), 5.79 (s, 1H, O-CH-O), 4.05–4.13 (m, 4H, -OCH_2-CH_2O-); 7.39–8.33 (m, 11H, Aromatic H & -N = CH), 9.93 (1H, s, -NH); ^{13}C NMR (δ, 125 MHz, DMSO-d_6, Me_4Si) 22.89 (-CH_3), 67.44 (-OCH_2-CH_2O-), 105.33 (O-CH-O), 126.74, 127.21, 127.29, 130.23, 130.33, 133.68, 136.86, 139.26, 136.44, 142.67 (Ar C) 148.22 (-N = CH), 152.55 (-C = N), 161.42 (-C = O-N=), 163.98 (-C = O-NH); MS: m/z 612.21, 614.30, 616.10 (M+), (M + 2), (M + 4). Analysis for $C_{26}H_{20}N_4O_4Br_2$, (612.27) Calcd: % C 51.00; H 3.29; N 9.15. Found: % C 51.02; H 3.27; N 9.17

*4-(2-phenyl-4-oxo-(3H) quinazolin-3-yl)-benzoic acid (4-[1, 3]dioxolan-2ylbenzyliden) hydrazide (**6d**)*

Yield: 85 %, mp >240 °C; IR (KBr, υ cm^{-1}): 1658 (-C = O cyclic tertiary amide), 1682, 1538 (-C = O Acyclic secondary amide), 3312, 3189 (-NH-), 1641 (CH = N); ^{1}H NMR (δ, 400 MHz, DMSO-d_6, Me_4Si) 4.11–4.20 (m, 4H, -OCH_2-CH_2O-), 5.81 (s, 1H, O-CH-O), 7.51–8.29 (m, 18H, Aromatic H & -N = CH), 10.91 (1H, s, -NH); ^{13}C NMR (δ, 125 MHz, DMSO-d_6, Me_4Si) 67.44 (-OCH_2-CH_2O-), 105.52 (O-CH-O), 122.07, 122.99, 125.18, 126.29, 126.74, 127.12, 127.27, 128.07, 128.68, 130.13, 130.57, 131.41, 131.73, 133.68, 135.48, 139.99, 142.67, 146.02 (Ar C) 148.17 (-N = CH), 152.19 (-C = N), 163.11 (-C = O-N=), 163.79; (-C = O-NH); MS: m/z 516.50 (M+). Analysis for $C_{31}H_{24}N_4O_4$, (516.55) Calcd: % C,72.08; H, 4.68; N, 10.85. Found:% C,72.10; H, 4.66; N, 10.84.

*4-(6-bromo-2-phenyl-4-oxo-(3H) quinazolin-3-yl)-benzoic acid (4-[1, 3]dioxolan-2-yl benzyliden) hydrazide (**6e**)*

Yield: 83 %, mp >240 °C; IR (KBr, υ cm^{-1}): 1655 (-C = O cyclic tertiary amide), 1684,1535 (-C = O Acyclic secondary amide), 3412, 3228 (-NH-), 1642 (CH = N); ^{1}H NMR (δ, 400 MHz, DMSO-d_6, Me_4Si) 3.97–4.15 (m, 4H, -OCH_2-CH_2O-), 5.81 (s, 1H, O-CH-O), 7.43–8.41 (m, 17H, Aromatic H & -N = CH), 9.97 (1H, s, -NH); ^{13}C NMR (δ, 125 MHz, DMSO-d_6, Me_4Si), 67.57 (-OCH_2-CH_2O-), 105.47 (O-CH-O), 118.84, 122.07, 126.74, 127.27, 127.62, 127.90, 128.07, 128.68, 130.13, 130.57, 131.41, 131.73, 133.68, 134.20, 135.48, 139.99, 142.67, 145.27 (Ar C) 148.13 (-N = CH), 152.20 (-C = N), 163.03 (-C = O-N=), 163.83; (-C = O-NH); MS: m/z 595.41, 597.35 (M+), (M + 2). Analysis for $C_{31}H_{23}N_4O_4Br$, (595.44) Calcd: % C,62.53; H, 3.89; N, 9.41. Found:% C,62.54; H, 3.88; N, 9.42.

*4-(6,8-dibromo-2-phenyl-4-oxo-(3H)quinazolin-3-yl)-benzoic acid (4-[1, 3]dioxolan-2yl benzyliden) hydrazide (**6f**)*

Yield: 80 %, mp >240 °C; IR (KBr, υ cm^{-1}): 1652 (-C = O cyclic tertiary amide), 1677,1530 (-C = O Acyclic secondary amide), 3399, 3185(-NH-), 1637 (CH = N); ^{1}H NMR (δ, 400 MHz, DMSO-d_6, Me_4Si) 4.04–4.12 (m, 4H, -OCH_2-CH_2O-), 5.77 (s, 1H, O-CH-O), 7. 41–8.36 (m, 16H, Aromatic H & -N = CH), 9.89 (1H, s, -NH); ^{13}C NMR (δ, 125 MHz, DMSO-d_6, Me_4Si), 67.57 (-OCH_2-CH_2O-), 105.48 (O-CH-O), 116.75, 122.07, 122.19, 125.56, 126.62, 126.73, 127.26, 128.06, 128.67, 130.56, 131.41, 131.73, 133.68, 135.47, 136.38, 137.32, 139.98, 142.67, 148.27, 152.34 (Ar C) 148.25 (-N = CH), 152.30 (-C = N), 163.63 (-C = O-N=), 163.87; (-C = O-NH); MS: m/z 674.28, 676.29, 678.22 (M+), (M + 2), (M + 4). Analysis for $C_{31}H_{22}N_4O_4Br_2$, (674.34) Calcd: % C,55.21; H, 3.29; N, 8.31. Found:% C,55.22; H, 3.31; N, 8.32.

*General procedure for the synthesis of 4-(substituted-4-oxo-(3H) quinazolin-3-yl)–benzoic acid (4-formyl-benzylidene) hydrazide (**7a–f**)*

The synthesis was carried out by following a similar method reported earlier [7]. 4.51 g (0.01 mol^{-1}) of compound **6a** was mixed with a solution of 3 mL perchloric acid in 50 mL 1,4-dioxane. The mixture was stirred at room temperature for 12 h. The solution was diluted with chloroform (30 mL) and washed with a saturated solution of sodium bicarbonate. The organic layer was separated and dried over anhydrous Na_2SO_4. The solvent was removed in vacuo and the light yellow solid residue was subjected to column chromatography in toluene: methanol (5:1) to get as light yellow solid product **7a.** In a similar way all other products **7b–f** were obtained by the above procedure.

*4-(2-methyl-4-oxo-(3H) quinazolin-3-yl)–benzoic acid (4-formyl-benzylidene) hydrazide (**7a**)*

Yield: 79 %, mp >240 °C; IR (KBr υ cm^{-1}): 1649 (-C = O cyclic tertiary amide), 1705, 1535 (-C = O Acyclic secondary amide), 3351, 3198 (-NH-), 1639 (-C = N); ^{1}H NMR (d, 400 MHz, DMSO-d_6, Me_4Si)

2.40 (s, 3H, CH_3), 7.41–8.23 (m, 13H, Ar-H, CH = N), 9.87 (s, 1H, -CHO), 10.05 (s, 1H, -NH); ^{13}C NMR (d, 125 MHz, DMSO-d_6, Me_4Si) 23.38 (-CH_3), 161.47(-C = O-N=), 163.93 (-C = O-NH), 148.27 (CH = N), 154.0(-C = N), 121.90, 121.96, 125.01, 126.35, 126.81, 127.18, 127.07, 129.04, 129.56, 130.23, 130.33, 131.55, 139.44, 139.44, 147.74, 191.17 (CHO); MS: m/z 410.00 (M+). Analysis for $C_{24}H_{18}N_4O_3$, (410.42) Calcd: % C, 70.23; H, 4.42; N, 13.65. Found: % C, 70.23; H, 4.44; N, 13.67.

*4-(2-methyl-6-bromo-4-oxo-(3H) quinazolin-3-yl)-benzoic acid (4-formyl-benzylidene) hydrazide (***7b***)*

Yield: 82 %, mp >240 °C; IR (KBr υ cm^{-1}): 1654 (-C = O cyclic tertiary amide), 1699, 1531 (-C = O Acyclic secondary amide), 3348, 3190 (-NH-), 1638 (-C = N); ^{1}H NMR (d, 400 MHz, DMSO-d_6, Me_4Si) 2.48 (s, 3H, CH_3), 7.44–8.36 (m, 12H, Ar-H, CH = N), 9.99 (s, 1H, -CHO), 10.05 (s, 1H, -NH); ^{13}C NMR (d, 125 MHz, DMSO-d_6, Me_4Si) 23.33 (-CH_3), 161.02 (-C = O-N=), 163.93 (-C = O-NH), 148.27 (CH = N), 154.0(-C = N), 116.99, 121.96, 127.19, 127.34, 127.38, 128.26, 129.06, 130.23, 130.33, 131.45, 131.55, 139.44, 139.66, 146.74, 191.14 (CHO); MS: m/z 489.20, 491.20 (M+), (M + 2). Analysis for $C_{24}H_{17}BrN_4O3$, (489.32) Calcd: % C, 58.91; H, 3.50; N, 11.63. Found:% C, 58.91; H, 3.50; N, 11.63.

*4-(2-methyl-6,8-dibromo-4-oxo-(3H)quinazolin-3-yl)-benzoic acid (4-formyl-benzylidene) hydrazide (***7c***)*

Yield: 78 %, mp >240 °C; IR (KBr υ cm^{-1}): 1647 (-C = O cyclic tertiary amide), 1702, 1529 (-C = O Acyclic secondary amide), 3341, 3188 (-NH-), 1641 (-C = N); ^{1}H NMR (d, 400 MHz, DMSO-d_6, Me_4Si) 2.39 (s, 3H, CH_3), 7.39–8.33 (m, 11H, Ar-H, CH = N), 9.93 (s, 1H, -CHO), 10.01 (s, 1H, -NH); ^{13}C NMR (d, 125 MHz, DMSO-d_6, Me_4Si) 23.33 (-CH_3), 161.49 (-C = O-N=), 163.93 (-C = O-NH), 148.27 (CH = N), 152.55 (-C = N), 114.75, 120.07, 121.19, 125.56, 127.73, 127.26, 129.67, 130.56, 131.41, 131.73, 136.68, 139.47, 139.38, 139.32, 139.98 191.16 (CHO); MS: m/z 568.20, 570.20, 572.20 (M+),(M + 2) (M + 4). Analysis for $C_{24}H_{16}Br_2N_4O_3$, (568.22) Calcd: % C, 50.73; H, 2.84; N, 9.86. Found:%% C, 50.75; H, 2.86; N, 9.88.

*4-(2-phenyl-4-oxo-(3H) quinazolin-3-yl)-benzoic acid (4-formyl-benzylidene) hydrazide (***7d***)*

Yield: 85 %, mp >240 °C; IR (KBr, υ cm^{-1}): 1657 (-C = O cyclic tertiary amide), 1694, 1535 (-C = O Acyclic secondary amide), 3300, 3190 (-NH-), 1640 (-C = N); ^{1}H NMR (d, 400 MHz, DMSO-d_6, Me_4Si) 7.42–8.29 (m, 18H, Ar-H, CH = N), 9.89 (s, 1H, -CHO), 10.91 (s, 1H, -NH); ^{13}C NMR (d, 125 MHz, DMSO-d_6, Me_4Si) 152.19 (CH = N), 163.74,(-C = O-N=), 163.93 (-C = O-NH), 122.07, 122.99, 125.17, 126.29, 127.19, 128.07, 128.68, 129.07, 130.57, 131.41, 131.55, 131.73, 135.48, 139.66, 139.99, 146.03. 191.18 (CHO); MS: m/z 472.00 (M+). Analysis for $C_{29}H_{20}N_4O_3$, (472.49) Calcd: % C,73.72; H, 4.27; N, 11.86. Found:% C,73.72; H, 4.27; N, 11.85.

*4-(2-phenyl-6-bromo-4-oxo-(3H) quinazolin-3-yl)-benzoic acid (4-formyl-benzylidene) hydrazide (***7e***)*

Yield: 76 %, mp >240 °C; IR (KBr, υ cm^{-1}): 1655 (-C = O cyclic tertiary amide), 1705, 1532 (-C = O Acyclic secondary amide), 3350, 3199 (-NH-), 1640 (-C = N); ^{1}H NMR (d, 400 MHz, DMSO-d_6, Me_4Si) 7.43–8.41 (m, 17H, Ar-H, CH = N), 9.97 (s, 1H, -CHO), 9.91 (s, 1H, -NH); ^{13}C NMR (d, 125 MHz, DMSO-d_6, Me_4Si) 152.19 (CH = N), 163.03 (-C = O-N=), 163.93 (-C = O-NH), 118.84, 122.07, 122.99, 125.17, 126.29, 127.19, 128.07, 128.68, 129.07, 130.57, 121.41, 131.55, 131.73, 135.48, 139.66, 139.99, 146.03, 192.11 (CHO); MS: m/z 551.12, 553.31 (M+), (M + 2). Analysis for $C_{29}H_{19}BrN_4O_3$, (551.39) Calcd: % C, 63.17; H, 3.47; N, 10.16. Found:% C, 65.18; H, 3.49; N, 10.18.

*4-(2-phenyl-6,8-dibromo-4-oxo-(3H)quinazolin-3-yl)-benzoic acid (4-formyl-benzylidene) hydrazide (***7f***)*

Yield: 83 %, mp >240 °C; IR (KBr, υ cm^{-1}): 1641 (-C = O cyclic tertiary amide), 1705, 1532 (-C = O Acyclic secondary amide), 3347, 3189 (-NH-), 1639 (-C = N); ^{1}H NMR (d, 400 MHz, DMSO-d_6, Me_4Si) 7.42–8.86 (m, 16H, *J*=8.5 Hz, Ar-H), 9.88 (s, 1H, -CHO), 9.89 (s, 1H, -NH), ^{13}C NMR (d, 125 MHz, DMSO-d_6, Me_4Si) 152.43 (CH = N), 163.84,(-C = O-N=), 163.93 (-C = O-NH), 116.75,, 122.07, 122.19, 125.56, 126.62, 126.73, 127.26, 128.06, 128.67, 130.56, 131.41, 131.41, 131.73, 133.68, 135.47, 136.38, 137.32, 139.98, 142.67, 191.11 (CHO); MS: m/z 630.14, 632.15, 634.15 (M+). Analysis for $C_{29}H_{18}Br_2N_2O_4$, (630.29) Calcd: % C, 55.26; H, 2.88; N, 8.89. Found:% C, 55.26; H, 2.88; N, 8.89.

*General procedure for the synthesis of fulleropyrrolidines (***8a–f***)*

The synthesis was carried out following a method similar to that reported earlier [50]. Schiff base **7a** (41.0 mg, 0.1 mmol), N-methylglycine (5 mg) and C_{60} (72 mg, 0.1 mmol) were refluxed in dry toluene in inert atmosphere for 6 h. The product was first purified by column chromatography (toluene/ethyl acetate 9:1) to obtain pure product **8a.** All other products (**8b–f**) were obtained by a similar procedure.

Compound **8a**

Yield: 38 %, mp >240 °C; IR (KBr, υ cm^{-1}) 3410, 3300 (N–H), 3148, (Ar–H), 1648 (-C = O cyclic tertiary amide) 1700, 1536 (-C = O acyclic secondary amide), 1640 (C = N), 527 (organo fullerene); ^{1}H NMR (d, 500 MHz, $CDCl_3$): 7.46–8.20 (m, 13H, Ar–H, CH = N), 4.25 (dd, 1H, *J*=9.3, HHC–N of the pyrrolidine ring), 3.61 (dd, 1H, *J*=9.3, HHC–N of the pyrrolidine ring), 4.51 (s, 1H, CH of the pyrrolidine ring), 9.93 (s, 1H, NH), 2.21 (s, 3H, CH_3 linked to N of pyrrolidine ring), 2.45 (s, 3H, CH_3 of quinazoline ring); ^{13}C NMR (d, 125 MHz, $CDCl_3$) 163.66, (C = O of quinazoline ring), 160.64 (CONH), 154.32, 151.43, 150.52, 147.91, 146.81, 145.94, 143.24, 143.23, 142.35, 142.23, 141.18, 140.82, 135.94, 134.22, 133.13, 131.40, 129.23, 128.95, 128.03, 127.62, 126.63, 125.08, 124.06, 123.48, 122.85, 118.93, 14.41, 112.63, 110.40, 28.28 (quinazoline ring CH_3), 40.25 (CH_3 linked to N of the pyrrolidine ring), 69.21 (NCH_2 of pyrrolidine ring), 83.31 (NCH of the pyrrolidine ring), 77.22 73.50 (sp3 C– of C_{60}), 72.73, 72.43, 68.65 (sp3 C– of C_{60}); ESI m/z: 1158.00 (M+). Analysis for $C_{86}H_{23}N_5O_2$, (1158.14).

Compound **8b**

Yield: 37 %, mp >240 °C; IR (KBr, υ cm^{-1}) 3418, 3190 (N–H), 1652 (-C = O cyclic tertiary amide) 1698, 1535 (-C = O acyclic secondary amide), 1640 (C = N), 526 (organo fullerene); ^{1}H NMR (d, 500 MHz, $CDCl_3$): 7.43–8.37 (m, 12H, Ar–H, CH = N), 4.25 (dd, 1H, *J*=9.6, HHC–N of the pyrrolidine ring), 3.62 (dd, 1H, *J*=9.6, HHC–N of the pyrrolidine ring), 4.58 (s, 1H, CH of the pyrrolidine ring), 10.12 (s, 1H, NH), 2.25 (s, 3H, CH3 linked to N of pyrrolidine ring), 2.52 (s, 3H, CH_3 of quinazoline ring); ^{13}C NMR (d, 125 MHz, $CDCl_3$) 163.64, (C = O of quinazoline ring), 161.64 (CONH), 153.82, 151.63, 150.55, 146.98, 146.86, 145.94, 143.29, 143.06, 142.22, 142.03, 141.21, 140.81, 135.93, 134.21, 133.44, 130.65, 129.22, 128.77, 128.20, 127.64, 126.68, 125.45, 124.21, 123.52, 121.81, 118.91, 114.34, 112.63, 111.42, 28.82 (quinazoline ring CH_3), 40.58 (CH_3 linked to N of the pyrrolidine ring), 67.25 (NCH_2 of pyrrolidine ring), 82.23 (NCH of the pyrrolidine ring), 77.44 73.50 (sp^3 C– of C_{60}), 72.76, 72.44, 68.62 (sp^3 C– of C_{60}); ESI m/z: 1237.10, 1239.20 (M+), (M + 2). Analysis for $C_{86}H_{22}BrN_5O_2$, (1237.03)

Compound **8c**

Yield: 33 %, mp >240 °C; IR (KBr, υ cm^{-1}) 3450, 3256 (N–H), 1650 (C = N); 1645 (-C = O cyclic tertiary amide) 1707, 1529 (-C = O acyclic secondary amide), 1645 (C = N), 528 (organo fullerene); ^{1}H NMR (d, 500 MHz, $CDCl_3$): 7.38–8.32 (m, 11H, Ar–H, CH = N), 4.22 (dd, 1H, *J*=10.1, HHC–N of the pyrrolidine ring), 3.65 (dd, 1H, *J*=10.1, HHC–N of the pyrrolidine ring), 4.52 (s, 1H, CH of the pyrrolidine ring), 10.12 (s, 1H, NH), 2.19 (s, 3H, CH_3 linked to N of pyrrolidine ring), 2.41 (s, 3H, CH_3 of quinazoline ring); ^{13}C NMR (d, 125 MHz, $CDCl_3$) 163.62 (C = O of quinazoline ring), 160.64 (CONH), 154.34, 151.23, 150.56, 146.95, 146.85, 145.94, 143.54, 143.36, 142.36, 142.23, 141.16, 140.86, 135.93, 134.26, 133.46, 130.46, 129.23, 128.77, 128.24, 127.64, 126.63, 125.41, 124.26, 123.54, 122.84, 118.94, 14.46, 112.62, 111.42, 28.43 (quinazoline ring CH_3), 41.48 (CH_3 linked to N of the pyrrolidine ring), 67.28 (NCH_2 of pyrrolidine ring), 81.45 (NCH of the pyrrolidine ring), 77.25, 73.50 (sp^3 C– of C_{60}), 71.91, 72.43, 67.48 (sp^3 C– of C_{60}); ESI m/z: 1315.40, 1317.40, 1319.20, (M+), (M + 2), (M + 4). Analysis for $C_{86}H_{21}Br_2N_5O_2$, (1315.93).

Compound **8d**

Yield: 35 %, mp >240 °C; IR (KBr, υ cm^{-1}) 3410, 3300 (N–H), 1687 (C = N), 1645 (-C = O cyclic tertiary amide) 1695, 1535 (-C = O acyclic secondary amide), 1640 (C = N), 527 (organo fullerene); ^{1}H NMR (d, 500 MHz, $CDCl_3$): 7.41–8.23 (m, 18H, Ar–H, CH = N), 4.22 (dd, 1H, *J*=9.4, HHC–N of the pyrrolidine ring), 3.65 (dd, 1H, *J*=9.4 HHC–N of the pyrrolidine ring), 4.52 (s, 1H, CH of the pyrrolidine ring), 9.92 (s, 1H, NH), 2.28 (s, 3H, CH_3 linked to N of pyrrolidine ring); ^{13}C NMR (d, 125 MHz, $CDCl_3$) 163.24, (C = O of quinazoline ring), 162.15 (CONH), 154.12, 151.23, 150.52, 146.91, 146.81, 145.92, 143.24, 143.00, 142.32, 142.03, 141.11, 140.81, 135.93, 134.21, 133.43, 130.45, 129.23, 128.75, 128.20, 127.62, 126.65, 125.00, 124.06, 123.58, 122.80, 118.91, 14.43, 112.63, 111.40, 28.32 (quinazoline ring CH_3), 40.23 (CH_3 linked to N of the pyrrolidine ring), 67.63 (NCH_2 of pyrrolidine ring), 82.94 (NCH of the pyrrolidine ring), 77.20, 73.50 (sp^3 C– of C_{60}), 72.78, 72.42, 68.6 (sp^3 C– of C_{60}); ESI m/z: 1220.10 (M+). Analysis for $C_{91}H_{25}N_5O_2$, (1220.20).

Compound **8e**

Yield: 35 %, mp >240 °C; IR (KBr, υ cm^{-1}) 3420, 3235 (N–H), 2958, (Ar H), 1642 (-C = O cyclic tertiary amide) 1712, 1533 (-C = O acyclic secondary amide), 1677 (C = N), 526 (organo fullerene); ^{1}H NMR (d, 500 MHz, $CDCl_3$): 7.45–8.41 (m, 17H, Ar–H, CH = N), 4.21 (dd, 1H, *J*=9.4, HHC–N of the pyrrolidine ring), 3.68 (dd, 1H, *J*=9.4 HHC–N of the pyrrolidine ring), 4.51 (s, 1H, CH of the pyrrolidine ring), 9.97 (s, 1H, NH), 2.28 (s, 3H, CH_3 linked to N of pyrrolidine ring); ^{13}C NMR (d, 125 MHz, $CDCl_3$) 163.14, (C = O of quinazoline ring), 161.24 (CONH), 153.92, 151.33, 150.42, 146.96, 146.80, 145.93, 143.24, 143.32, 142.31, 142.33, 141.13, 140.61, 135.73, 134.25, 133.03, 130.46, 129.53, 128.75, 128.20, 127.67, 126.65, 125.30, 124.76, 123.55,

122.82, 118.94, 14.47, 112.63, 111.49, 28.34 (quinazoline ring CH_3), 40.23 (CH_3 linked to N of the pyrrolidine ring), 66.34 (NCH_2 of pyrrolidine ring), 81.26 (NCH of the pyrrolidine ring), 77.25 73.50 (sp^3 C– of C_{60}), 72.7, 72.47, 68.67 (sp^3 C– of C_{60}); ESI m/z: 1299.10, 1301.10 (M+), (M + 2). Analysis for $C_{91}H_{24}BrN_5O_2$, (1299.10).

Compound **8f**

Yield: 40 %, mp >240 °C; IR (KBr, υ cm^{-1}) 3429, 3320 (N–H), 3068, (Ar C–H), 1645 (-C = O cyclic tertiary amide) 1702, 1535 (-C = O acyclic secondary amide), 1675 (C = N), 524 (organo fullerene); ^{1}H NMR (d, 500 MHz, $CDCl_3$): 7.44–8.39 (m, 16H, Ar–H, CH = N), 4.23 (dd, 1H, *J*=9.6, HHC–N of the pyrrolidine ring), 3.62 (dd, 1H, *J*=9.6 HHC–N of the pyrrolidine ring), 4.52 (s, 1H, CH of the pyrrolidine ring), 9.96 (s, 1H, NH), 2.22 (s, 3H, CH_3 linked to N of pyrrolidine ring); ^{13}C NMR (d, 125 MHz, $CDCl_3$) 163.43 (C = O of quinazoline ring), 161.65 (CONH), 154.32, 151.24, 150.54, 146.93, 146.83, 145.96, 143.44, 143.23, 142.42 142.23, 141.13, 140.81, 135.98, 134.25, 133.65 130.46, 129.27, 128.74, 128.22, 127.62, 126.64, 125.03, 124.26, 123.51, 122.85, 118.93, 14.47, 112.66, 111.44, 28.37 (quinazoline ring CH_3), 40.28 (CH_3 linked to N of the pyrrolidine ring), 69.29 (NCH_2 of pyrrolidine ring), 83.23 (NCH of the pyrrolidine ring), 77.26 73.50 (sp^3 C– of C_{60}), 72.7, 72.43, 68.65 (sp^3 C– of C_{60}); ESI m/z: 1378.00 1380.10 1382.30 (M+). Analysis for $C_{91}H_{23}Br_2N_5O_2$, (1378.00).

*General procedure for the synthesis of fullerene-N,N-dimethylpyrrolidines iodide salt (fullerene-quinazolinone conjugates) (***9a–f***)*

A solution of fulleropyrrolidine derivative **8a** (80 mg, 0.0691 mmol) and iodomethane (9.8 mg, 0.0691) was refluxed with stirring for 2 days under argon. The residue was then washed with toluene (three times) and hexane (twice). The solvent was removed under vacuum to give fullerene-N-dimethylpyrrolidine iodide salts (**9a**) as a brownish solid. All other products **9b–f** were obtained by a similar procedure

Compound **9a**

Yield: 98 %, mp 212 °C; IR (KBr, υ cm^{-1}) 3410, 3300 (N–H), 3148, (Ar–H), 2945 (N- CH_3) 1701, 1540 (-C = O acyclic secondary amide), 1643 (-C = O cyclic tertiary amide), 1600 (C = N), 525 (organo fullerene); ^{1}H NMR (d, 500 MHz, $CDCl_3$): 7.46–8.20 (m, 13H, Ar–H, CH = N), 4.25 (dd, 1H, *J*=9.3, HHC–N of the pyrrolidine ring), 3.61 (dd, 1H, *J*=9.3, HHC–N of the pyrrolidine ring), 4.51 (s, 1H, CH of the pyrrolidine ring), 9.93 (s, 1H, NH), 2.21 (s, 3H, CH3 linked to N of pyrrolidine ring), 2.30 (s, 3H, CH_3 linked to N of pyrrolidine ring), 2.45 (s, 3H, CH_3 of quinazoline ring); ^{13}C NMR (d, 125 MHz, $CDCl_3$) 163.62 (C = O of quinazoline ring), 160.66 (CONH), 154.11, 151.20, 150.54, 146.96, 146.83, 145.94, 143.25, 143.00, 142.32, 142.03, 141.11, 140.81, 135.93, 134.21, 133.43, 130.45, 129.23, 128.75, 128.26, 127.67, 126.67, 125.03, 124.06, 123.56, 122.84, 118.93, 14.45, 112.67, 111.42, 28.33 (quinazoline ring CH_3), 42.54, 41.83 ((CH_3)$_2$ linked to N of the pyrrolidine ring), 69.22 (NCH_2 of pyrrolidine ring), 83.16 (NCH of the pyrrolidine ring), 77.26 73.50 (sp^3 C– of C_{60}), 72.73, 72.45, 68.66 (sp3 C– of C_{60}); ESI m/z: 1173.20 (M+). Analysis for $C_{87}H_{26}IN_5O_2$, (1300.07)

Compound **9b**

Yield: 97 %, mp >240 °C; IR (KBr, υ cm^{-1}) 3410, 3204 (N–H), 3140, (Ar–H), 2945 (N-CH_3) 1701, 1536 (-C = O acyclic secondary amide), 1654 (-C = O cyclic tertiary amide), 1660 (C = N), 526 (organo fullerene); ^{1}H NMR (d, 500 MHz, $CDCl_3$): 7.46−8.20 (m, 12H, Ar–H, CH = N), 4.25 (dd, 1H, *J* =9.6, HHC–N of the pyrrolidine ring), 3.62 (dd, 1H, *J*=9.6, HHC–N of the pyrrolidine ring), 4.58 (s, 1H, CH of the pyrrolidine ring), 10.12 (s, 1H, NH), 2.25 (s, 3H, CH3 linked to N of pyrrolidine ring), 2.32 (s, 3H, CH_3 linked to N of pyrrolidine ring), 2.52 (s, 3H, CH_3 of quinazoline ring); ^{13}C NMR (d, 125 MHz, $CDCl_3$) 163.64 (C = O of quinazoline ring), 160.59 (CONH), 154.14, 151.22, 150.54, 146.93, 146.83, 145.94, 143.26, 143.02, 142.33, 142.05, 141.13, 140.82, 135.95, 134.25, 133.45, 130.47, 129.26, 128.77, 129.20, 127.64, 126.67, 125.03, 124.05, 123.56, 122.88, 118.95, 14.42, 112.67, 111.46, 28.34 (quinazoline ring CH_3), 39.54, 41.48 ((CH_3)$_2$ linked to N of the pyrrolidine ring), 67.43 (NCH_2 of pyrrolidine ring), 82.45 (NCH of the pyrrolidine ring), 77.24 73.50 (sp3 C– of C_{60}), 72.77, 72.44, 68.62 (sp^3 C– of C_{60}); ESI m/z: 1252.40 1254.50 (M+), (M + 2). Analysis for $C_{87}H_{25}BrIN_5O_2$, (1378.97).

Compound **9c**

Yield: 98 %, mp 214 °C; IR (KBr, υ cm^{-1}) 3450, 3256 (N–H), 3116, (Ar–H), 2840 (N-CH_3) 1705, 1535 (-C = O acyclic secondary amide), 1657 (-C = O cyclic tertiary amide), 1665 (C = N), 528 (organo fullerene); ^{1}H NMR (d, 500 MHz, $CDCl_3$): 7.38–8.32 (m, 11H, Ar–H, CH = N), 4.22 (dd, 1H, *J*=10.1, HHC–N of the pyrrolidine ring), 3.65 (dd, 1H, *J*=10.1, HHC–N of the pyrrolidine ring), 4.52 (s, 1H, CH of the pyrrolidine ring), 10.12 (s, 1H, NH), 2.19 (s, 3H, CH3 linked to N of pyrrolidine ring), 2.23 (s, 3H, CH_3 linked to N of pyrrolidine ring), 2.41 (s, 3H, CH_3 of quinazoline ring); ^{13}C NMR (d, 125 MHz, $CDCl_3$) 161.22 (C = O of quinazoline ring), 162.45 (CONH),

154.22, 151.21, 150.54, 146.96, 146.83, 145.95, 143.24, 143.11, 142.35, 142.23, 141.43, 140.36, 135.65, 134.55, 133.83, 130.65, 129.29, 128.74, 128.22, 127.64, 126.66, 125.08, 124.26, 123.59, 122.80, 118.95, 14.43, 112.73, 111.45, 28.39 (quinazoline ring CH_3), 41.2, 40.5 ($(CH_3)_2$ linked to N of the pyrrolidine ring), 67.51 (NCH_2 of pyrrolidine ring), 81.42 (NCH of the pyrrolidine ring), 77.21 73.50 (sp^3 C– of C_{60}), 72.75, 72.45, 68.66 (sp3 C– of C_{60}); ESI m/z: 1330.50, 1332.30, 1334.50 (M+), (M + 2), (M + 4). Analysis for $C_{87}H_{24}Br_2IN_5O_2$, (1457.87).

Compound **9d**

Yield: 94 %, mp 218 °C; IR (KBr, υ cm^{-1}) 3415, 3300 (N–H), 3128, (Ar–H), 2840, 2740 (N-CH_3), 1701, 1537 (-C = O acyclic secondary amide), 1653 (-C = O cyclic tertiary amide), 1654 (C = N), 524 (organo fullerene);); ^{1}H NMR (d, 500 MHz, $CDCl_3$): 7.41–8.23 (m, 18H, Ar–H, CH = N), 4.22 (dd, 1H, *J*=9.4, HHC–N of the pyrrolidine ring), 3.65 (dd, 1H, *J*=9.4 HHC–N of the pyrrolidine ring), 4.52 (s, 1H, CH of the pyrrolidine ring), 9.92 (s, 1H, NH), 2.28 (s, 3H, CH3 linked to N of pyrrolidine ring), 2.35 (s, 3H, CH_3 linked to N of pyrrolidine ring); ^{13}C NMR (d, 125 MHz, $CDCl_3$) 161.25 (C = O of quinazoline ring), 164.65 (CONH), 154.28, 151.28, 150.32, 146.87, 146.89, 145.94, 143.27, 143.12, 142.34, 142.13, 141.17, 140.84, 135.83, 134.25, 133.73, 130.44, 129.28, 128.73, 128.28, 127.52, 126.62, 125.26, 124.45, 123.57, 122.88, 118.71, 14.49, 112.64, 111.46, 38.29, 40.55 ($(CH_3)_2$ linked to N of the pyrrolidine ring), 69.71 (NCH_2 of pyrrolidine ring), 83.00 (NCH of the pyrrolidine ring), 77.23 73.50 (sp3 C– of C_{60}), 72.71, 72.44, 68.60 (sp^3 C– of C_{60}); ESI m/z: 1235.60 (M+). Analysis for $C_{92}H_{28}IN_5O_2$, (1362.13).

Compound **9e**

Yield: 97 %, mp 212 °C; IR (KBr, υ cm^{-1}) 3420, 3235 (N–H), 2958, (Ar H), 2850 (N-CH_3), 1726, 1536 (-C = O acyclic secondary amide), 1658 (-C = O cyclic tertiary amide), 1647 (C = N), 527 (organo fullerene); ^{1}H NMR (d, 500 MHz, $CDCl_3$): 7.45–8.41 (m, 17H, Ar–H, CH = N), 4.21 (dd, 1H, *J*=9.4, HHC–N of the pyrrolidine ring), 3.68 (dd, 1H, *J*=9.4 HHC–N of the pyrrolidine ring), 4.51 (s, 1H, CH of the pyrrolidine ring), 9.97 (s, 1H, NH), 2.28 (s, 3H, CH3 linked to N of pyrrolidine ring), 2.30 (s, 3H, CH_3 linked to N of pyrrolidine ring); ^{13}C NMR (d, 125 MHz, $CDCl_3$) 161.32 (C = O of quinazoline ring), 164.64 (CONH), 154.12, 151.23, 150.52, 146.91, 146.81, 145.92, 143.24, 143.00, 142.32, 142.03, 141.14, 140.88, 135.83, 134.27, 133.46, 130.55, 129.25, 128.85, 128.24, 127.63, 126.25, 125.30, 124.08, 123.52, 122.81, 118.91, 14.42, 112.66, 111.42, 39.25, 42.52 ($(CH_3)_2$ linked to N of the pyrrolidine ring), 66.22 (NCH_2 of pyrrolidine ring), 81.40 (NCH of the pyrrolidine ring), 77.22 73.50 (sp3 C– of C_{60}), 72.70, 72.45, 68.66 (sp3 C– of C_{60}); ESI m/z: 1314.40, 1316.20 (M+) (M + 2). Analysis for $C_{92}H_{27}BrIN_5O_2$, (1441.04).

Compound **9f**

Yield: 98 %, mp 210 °C; IR (KBr, υ cm^{-1}) 3429, 3320 (N–H), 3068, (Ar C–H), 2921, (N-CH_3), 1715, 1533 (-C = O acyclic secondary amide), 1652 (-C = O cyclic tertiary amide), 1667 (C = N), 524 (organo fullerene); ^{1}H NMR (d, 500 MHz, $CDCl_3$): 7.44–8.39 (m, 16H, Ar–H, CH = N), 4.23 (dd, 1H, *J*=9.6, HHC–N of the pyrrolidine ring), 3.62 (dd, 1H, *J*=9.6 HHC–N of the pyrrolidine ring), 4.52 (s, 1H, CH of the pyrrolidine ring), 9.96 (s, 1H, NH), 2.22 (s, 3H, CH3 linked to N of pyrrolidine ring), 2.28 (s, 3H, CH_3 linked to N of pyrrolidine ring); ^{13}C NMR (d, 125 MHz, $CDCl_3$) 162.15 (C = O of quinazoline ring), 164.26 (CONH), 154.42, 151.22, 150.51, 146.98, 146.81, 145.92, 143.24, 143.11, 142.33, 142.33, 141.41, 140.85, 135.73, 134.27, 133.48, 130.35, 129.63, 128.77, 128.22, 127.52, 126.67, 125.29, 124.06, 123.63, 122.88, 118.99, 14.94, 112.63, 111.60, 28.42 (quinazoline ring CH_3), 40.4, 40.2 ($(CH_3)_2$ linked to N of the pyrrolidine ring), 69.2 (NCH_2 of pyrrolidine ring), 83.35 (NCH of the pyrrolidine ring), 77.25 73.50 (sp^3 C– of C_{60}), 72.71, 72.40, 68.63 (sp3 C– of C_{60}); ESI m/z: 1392.00, 1394.40, 1396.30 (M+), (M + 2), (M + 4) Analysis for $C_{92}H_{26}Br_2IN_5O_2$, (1519.94).

Preparation of **4a–f** and **5a–f** water suspensions

Aqueous suspensions of compounds **4a–f** and **5a–f** were prepared using a previously reported method [53]: 50 mg compound **4a** in 50 mL Milli-Q water was stirred at 40 °C for 2 weeks. The suspension thus obtained was filtered through a Whatmann filter, then through a 0.45-μm Osmonics nylon membrane and a 0.22-μm nylon membrane to remove aggregates larger than 200 nm. The water suspension obtained was then concentrated on a rotavapor to get different concentrations ranging from 1.562 to 2,000 μg/mL.

In vitro evaluation of antimycobacterial activity

The compounds were screened for in vitro antimycobacterial activity against *Mycobacterium tuberculosis* ($H_{37}Rv$) using the LJ (Lowenstein and Jensen) minimal inhibitory concentration (MIC) method [54]. Stock solutions of primary 1000, 500, 250 and secondary 200, 100, 62.5, 50, 25, 12.5, 6.25, 3.25, 1.562 μg/mL dilutions of each test compound in DMSO (dimethyl sulfoxide) were added to liquid LJ medium and the resulting media were sterilized by the inspissation method. A culture of *M. tuberculosis* $H_{37}Rv$ growing on LJ medium was harvested in 0.85 %

saline in bijou bottles. These tubes were then incubated at 37 °C for 24 h followed by streaking of *M. tuberculosis* $H_{37}Rv$ (5×104 bacilli per tube). These tubes were then incubated at 37 (± 1) °C. Growth of bacilli was seen after 12 days, 22 days and finally 28 days of incubation. Tubes with test compounds were compared with control tubes where medium alone was incubated with *M. tuberculosis* $H_{37}Rv$. The concentration at which no development of colonies occurred or <20 colonies was taken as the MIC concentration of the test compound. The standard strain *M. tuberculosis* $H_{37}Rv$ was also tested with known drugs isoniazid and rifampicin.

Computational details

Sequence alignment and secondary structure comparison

Homologous proteins of *M. tuberculosis* HGPRT were retrieved using a Blastp [34] search of the RCSB PDB [35] with the BLOSUM62 scoring matrix to identify templates for modeling. The best template was identified by its E value and sequence range. Modeling was executed in the ExPASy (Expert Protein Analysis System) Swiss Model program with specification of the chosen template.

Swiss Model [36] has four progressive stages to efficiently model protein structures. These include (1) template selection: selection of PDB coordinate structures files with quality indicators; (2) target template alignment: alignments are optimized by initially superimposing using an iterative least square algorithm, followed by a local pairwise alignment was performed and optimized with a heuristic approach; (3) model building: high scoring sequence similarities regions are first modeled, and loop assignments and modeling are performed using constraint space programming (CSP) and at a later stage, side chains are fixed using rotamer library; and (4) evaluation: the deviations in the generated model are settled by descent energy minimization using the GROMOS96 force field [55].

Disorderness predictions were carried out using the Disopred program [37] hosted by UCL to distinguish the regions of disordered structural profile, which in turn can be deployed in secondary structure alignment in order to remove spurious alignment between template and the input sequences.

Model validation and stereochemistry corrections

The modeled *M. tuberculosis* HGPRT was subjected to a standard energy minimization protocol using the AMBER92 ff99SB force field with 1,000 steps of steepest gradient optimization procedures in Chimera software [academic version]. AMBER92 ff99SB is a refined force field with the main emphasis on improvization of amino acids side-chain torsions (χ_1) [38]. The modeled protein was validated by Ramachandran plot [39] (stereochemistry check) and QMEAN [40] (quality measure). The model structure file was specified in the PROCHECK program available via the SAVES (Structural Analysis and Verification Server) server [56]. QMEAN6 Z-score was studied using QMEAN server for model quality estimation.

pK_a predictions

As the modeled *M. tuberculosis* HGPRT is known to contain charged residues, we calculated the pK_a values to understand the local environment of the residues at physiological pH and their H bonding potential. H++ works on standard generalized Born (GB) or the Poisson-Boltzmann (PB; considered in this study) methodology to compute pK_a values of ionizable residues. The analysis was carried out in an explicit solvent with endurance in dielectric ionic strength (internal 6, external 80, pH 6.5, salinity 0.15) with one Mg^{2+} counter-ion. A structure file was prepared with AMBER ff10 [57] topology descriptions and assignment of missing hydrogens.

Binding site prediction

It is well known that HGPRTs possess a catalytic site for enzymatic activity [42]. Q-SiteFinder was employed to identify ligand binding sites that utilize an interaction energy scheme to locate energetically favorable binding sites between the protein and a simple van der Waals probe [44]. A spatial proximal scheme was used to cluster energetically favorable sites and then ranked by accounting for estimated interaction energies. The top scoring predicted cavities were deployed in active site directed docking studies.

Molecular docking of fullerene derivatives and their energetic profile

Prior to docking, the ligand dataset was energy minimized using the Ghemical all-atom force field [45] engineered in the PyRx program [46] for the Scripps Research Institute. Docking simulations were performed on a single machine equipped with an Intel Dual-Core processor with 4 GB RAM and 150 GB hard disk operating on a Windows 7 operating system using iGEMDOCK version 2.1 program [47]. iGEMDOCK computes a ligand conformation and relative orientations owing to search space relative to the protein target binding site by applying genetic evolutionary methods (GA). Screening was carried out with the following specifications: population size = 500, number of generations = 100 and number of solutions = 10. Followed by generation of interaction profiles, the pharmacological interactions were mined and

assigned a Z score. We sorted the interaction profiles in the following order: binding energy, H bonding term and van der Waals term with electrostatic term remained undisturbed. The ligand–receptor interaction profile was further investigated using the PEARLS web program, which makes extensive use of the AMBER empirical force field [58] to estimate various energy descriptors [48].

Results and discussion

In vitro evaluation of the antimycobacterial activity of compounds **7a–f**, **8a–f** and **9a–f** along with the standard drugs is summarized in Table 1. A very pronounced enhancement in antimycobacterial activity can be seen upon attachment of the fullerene spheroid to the quinazolinone group.

The mycobacterium cell wall has a very high concentration of lipids and is associated with the resistance of these bacteria to stains and antibiotics. The waxy cell wall of these bacteria prevents the entry of molecules **7a–f** (250 μg/mL and 78 % inhibition); the only activity observed is due to the small amount probably entering through the porin pathway, like most antitubercular drugs [23]. However, upon accessorizing the molecule with a fullerene, **8a–f** can easily seep into the waxy cell wall, rupture it and facilitate the entry of the quinazolinone into the cytoplasm. Inside the cytoplasm, quinazolinone can easily cause cell death by inhibiting cell metabolism. Hence the MIC decreases to 6.25 μg/mL and inhibition increases to 93 %.

The introduction of a cationic charge results in better interaction between the carboxylic groups of mycolic acid present in the cell envelope of mycobacterium with derivatives **9a–f** (1.562 μg/mL and 98 % inhibition), resulting in better activity compared to **7a–f** and **8a–f**.

Table 1 In vitro antituberculosis activity and percentage inhibition against *Mycobacterium tuberculosis* $H_{37}Rv$ at concentration 250 μg/mL and minimum inhibitory concentration (MIC; μg/mL) of compounds **7a–f, 8a–f** and **9a–f**. *LJ* Lowenstein and Jensen. *DMSO* dimethylsulfoxide

Compound no.	LJ MIC method	
	MIC (μg/mL)	Inhibition (%) at 250 μg/mL
7a	250	78.12±1.21
7b	250	77.06±0.88
7c	200	79.07±0.91
7d	200	79.42±1.02
7e	200	79.55±1.23
7f	200	79.71±0. 42
8a	25	80.26±0.31
8b	12.5	89.02±1. 15
8c	12.5	91.11±0.99
8d	12.5	90.25±0.28
8e	6.25	92.07±1. 17
8f	6.25	93.08±1. 09
9a	3.125	90.01±1.32
9b	3.125	92.23±0.17
9c	3.125	95.45±1.23
9d	3.125	96.42±0.62
9e	3.125	98.12±1.23
9f	1.562	98.83±0.21
Isoniazid[a]	0.20	99.00
Rifampicine[a]	0.25	99.00
DMSO	–	–

[a] Standard drugs

Sequence alignment and secondary structure comparison

M. tuberculosis HGPRT is composed of 202 amino acids and has a phosphoribosyl transferase (PRT type I) domain [33]. A Blastp [34] search of the RCSB Protein Data Bank (PDB) [35] enabled us to identify the homologous proteins in various organisms. These include HGPRTs from *Thermoanaerobacter tengcongensis* (identity: 50.5 %; similarity: 71.3 %), *Bacillus anthracis* (46 %; 61.1 %), *Escherichia coli* (42.3 %; 60.1 %), *Salmonella typhimurium* (41.8 %; 59.6 %), *Vibrio cholerae* (41.5 %; 60.5 %), etc. Hence, we considered *T. tengcongensis* [PDB entry: 2geb, Expect (E) value for alignment: 1e-62] as a template for modeling the *M. tuberculosis* HGPRT using Swiss Model [36]. The structural features of the present model were discussed based on the template crystallographic and biological data.

Upon careful inspection of pairwise secondary structure alignment generated from template and *M. tuberculosis* HGPRT, all the structure assignments were proven to be consistent with the template and resembled the realistic protein structure (Fig. 3). The N-terminal 13 amino acids were not modeled due to the unavailability of alignment corresponding to the region, which represents merely a disordered structure profile. This disorderness was validated manually using UCL (University College London) Disopred program [37] and found to be correlated with the template in a confidence window of 8 and 9.

Model validation and stereochemistry corrections

The modeled *M. tuberculosis* HGPRT was energy minimized using the AMBER92 ff99SB [38] force field with 1,000 steps of steepest gradient optimization protocol to return a plausible model. Ramachandran plot [39] exhibited 91 % amino acids in core areas of φ-ψ distributions, with 9 % dispensed in additional allowed regions and no outliers

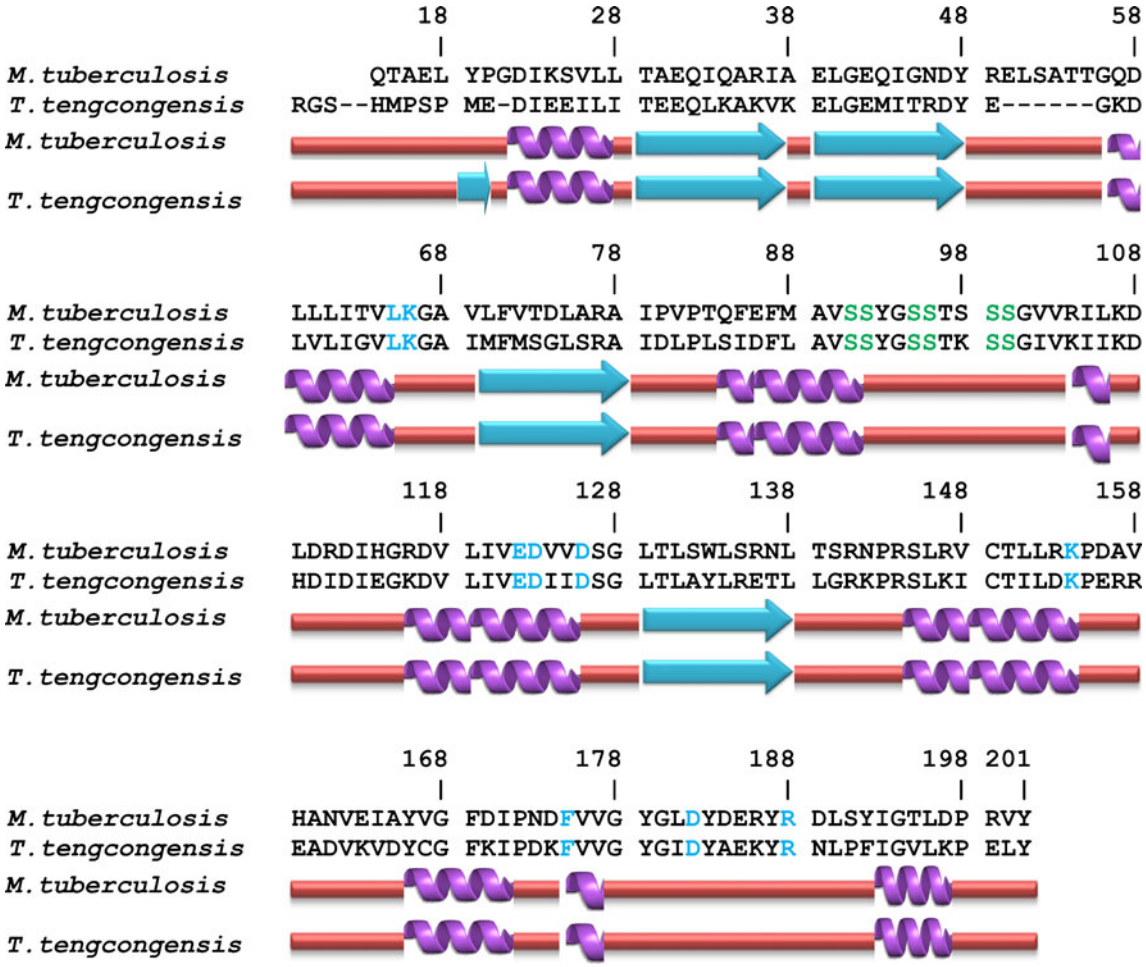

Fig. 3 Secondary structure alignment of Thermoanaerobacter tengcongensis (template) and *M.tuberculosis* (model) hypoxanthine-guanine phosphoribosyltransferases (HGPRTs). Active site residues and double serine repeat are highlighted in light blue and green. Secondary structure elements such as α-helices and β-sheets are represented in cyan and purple

(Fig. 4a). This stereochemistry quality measure can be compared to the template used. *T. tengcongensis* HGPRT reported 97.3 % in favorable regions, 2.7 % in additional allowed regions and no outliers. Besides, the QMEAN6 Z-score (a composite scoring function consisting of the following pseudo energy terms: C_β interaction, all-atom pairwise, solvation, torsional angle and agreement measures: secondary structure and solvent accessibility [40]) of the modeled HGPRT protein was observed to be 0.709, which is quite close to that of the experimental X-ray structures (Fig. 4b). Thus, the model was proved to be structurally realistic and was thus used for further analysis.

Structural features of modeled *M. tuberculosis* HGPRT

The active form of *T. tengcongensis* HGPRT exists in a dimer/tetramer form in solution [41]. Information from the monomeric template was utilized to identify the structurally conserved regions (SCRs) and active sites in the present model. *M. tuberculosis* HGPRT comprises three α-helices and nine β-sheets (Fig. 5). The hood domain consists of three β-sheets organized antiparallelly whereas the core domain is enclosed by a network of six β strands. Structural comparisons with other members revealed that four loops, designated by the Roman letters I, II, III and IV, actively participate in structural integrity of the enzyme. Loop I is known for its dimer interactions and exerts a strong influence on enzymatic efficiencies in an indirect fashion. It is also known as the PP_i (inorganic pyrophosphate) loop due to its binding affinity towards PP_i. Loop II is structurally annotated as a flexible loop due to its elasticity in bringing together the active site residues and oligomerization contacts—a prerequisite for stable conformation and enzymatic activity together with loop I. Loops III and IV supply amino acids to engage in substrate-binding and catalysis.

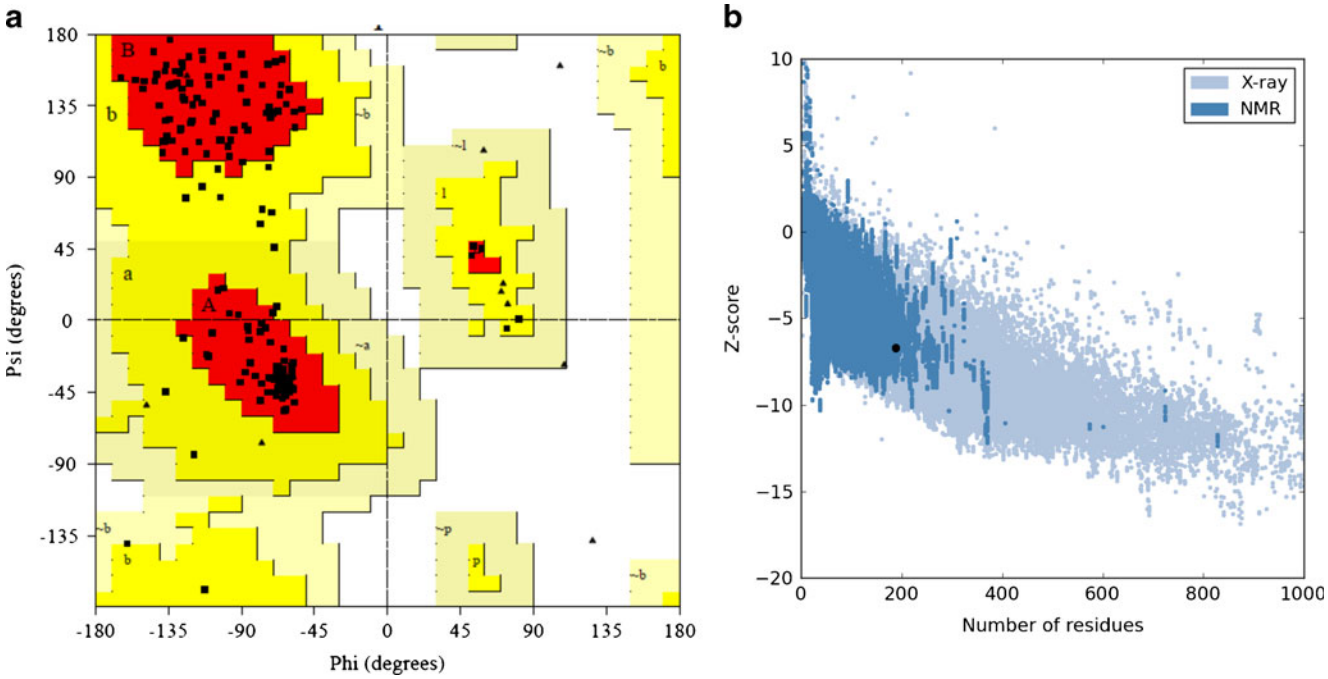

Fig. 4 **a** Ramachandran plot showing that amino acid distributions reflect a reliable structure. **b** Model quality (a black dot in the Z-score plot) resembles experimental structure statistics

Another structural feature in the modeled protein is its double serine repeat with the sequence pattern, SSXXSSXXSS at positions 91–100, forming an element of loop II. This feature is recognized for its thermostability activity. Chen and coworkers [42] proposed that this loop will undergo a large conformation upon binding to its substrate, α-D-phosphoribosyl-1-pyrophosphate (PRPP), thereby sealing off the active site cleft with the intention of shielding reactive transition species from the bulk solvent. It is also suggested that this loop will espouse a 3–10 helix conformation—a more stable structural form in contrast to the loop at the half closed position.

Structural comparison with the template revealed significant conservation at the active site enriched with positive and negatively charged residues. These include Leu65, Lys66, Glu122, Asp123, Asp126, Lys154, Phe175, Asp182 and Arg188. We believe that the occurrence of charged residues plays a vital role in catalysis at physiological pH. Theoretical pK_a values were calculated using the H++ program [43] by specifying the modeled protein as input. The predictions are as follows: Lys66 = 11.6, Glu122 = 6.8, Asp123 = 4.3, Asp126 = 1.2, Lys154 = 12.0, Asp182 = 1.3 and Arg188 = 12.0 making up a protein's total charge of −5 at pH 6.5. Of note, the active site residues are largely distributed in loops with close proximity to the core domain with extensions from the hood domain. Three-membered aromatic rings composed of Phe175, Tyr183 and Tyr 201 were observed to be oriented towards each other and seem to stabilize Phe175 for purine binding and catalysis in the present model, which is in good correspondence with the experimental structure of *T. tengcongensis* HGPRT proposed by Chen and coworkers [42].

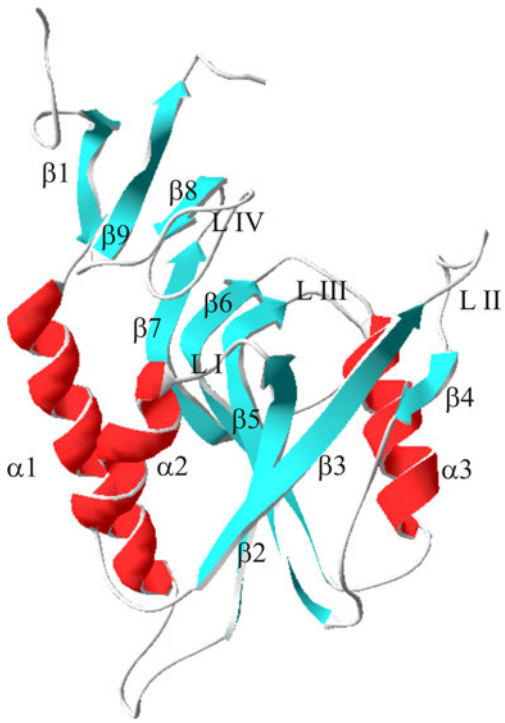

Fig. 5 The *M. tuberculosis* HGPRT model

Interaction of fullerene and its derivatives in M. tuberculosis HGPRT

A cavity with active site residues, along with adjacent neighbors within a proximity of 6 Å, was constructed to implement as a docking grid. A grid space with a site volume of 197 $Å^3$ predicted by Q-SiteFinder [44] was utilized in docking simulations. The ligand dataset consisted of six fullerene derivatives together with the parent compound. Fullerene was energy minimized using the Ghemical all-atom force field [45] and optimized by 1,000 steps of conjugate gradients protocol with the help of the PyRx program [46].

Active site directed docking studies were performed using iGEMDOCK version 2.1 [47]. We tried to investigate the specificity of the fullerene moiety initially to distinguish the floor within which to place the carbon cage in the vicinity of the active site and to allow the quinazolinone side arm to interact with active site residues. The fullerene cage prefers to interact with two floors encompassed by the following architecture: β1-β8-β9 and β5-β6-β7 (Fig. 6a). Upon examining the scoring function, the fullerene moiety appears to interact with non-covalent forces in the β1-β8-β9 structural arrangement with van der Waals term of -48.8825 kJ mol^{-1} overall contributing E_{total} of -49.9251 kJ mol^{-1}. Hence, it is evident that the major pharmacological activity of fullerene is its lipophilicity, as reflected by the major contribution of van der Waals term (97.91 %) to the total binding energy function.

The occupancy of the fullerene moiety on the structural floor adjacent to the active site was a crucial finding, and allows the quinazolinone moiety to interact with the active site residues (Fig. 6b). As the quinazolinone moiety is enriched with H bond acceptors, H bond donors and hydrophobic pharmacophore groups, and the active site possess chargeable amino acids, it is essential to understand these molecular interactions. Moreover, the preference of the quinazolinone moiety of fullerene to bind more to uncharged amino acids was observed, which can be distinguished into two main aspects: (1) We strongly believe that loops I and II are the chief protein folding unit that brings the active site residues close to each other compared to the crystallographic template data. Hence, we forsee that the H bond acceptors and donors of quinazolinone may participate in H bonding with active site amino acids along with its neighbors. (2) The aromatic pharmacophore of quinazolinone may aid in interaction, largely via π–π interactions with aromatic amino acids to flexibly place the aromatic ligand groups initially before optimizing its H bonding patterns. At first glance, we found that aliphatic amino acids interact better with H bond donors and acceptor groups of quinazolinone side arm. Then again, the aromatic moiety of the side arm prefers to interact with the aromatic hydrophobic side chains of cavity residues. The second prospect deals with π–π interactions, wherein the active site of *M. tuberculosis* HGPRT constitutes only one aromatic amino acid (Phe175) and, intriguingly, it is populated by charged residues, viz. Lys66, Glu122, Asp123, Asp126, Lys154, Asp182 and Arg188.

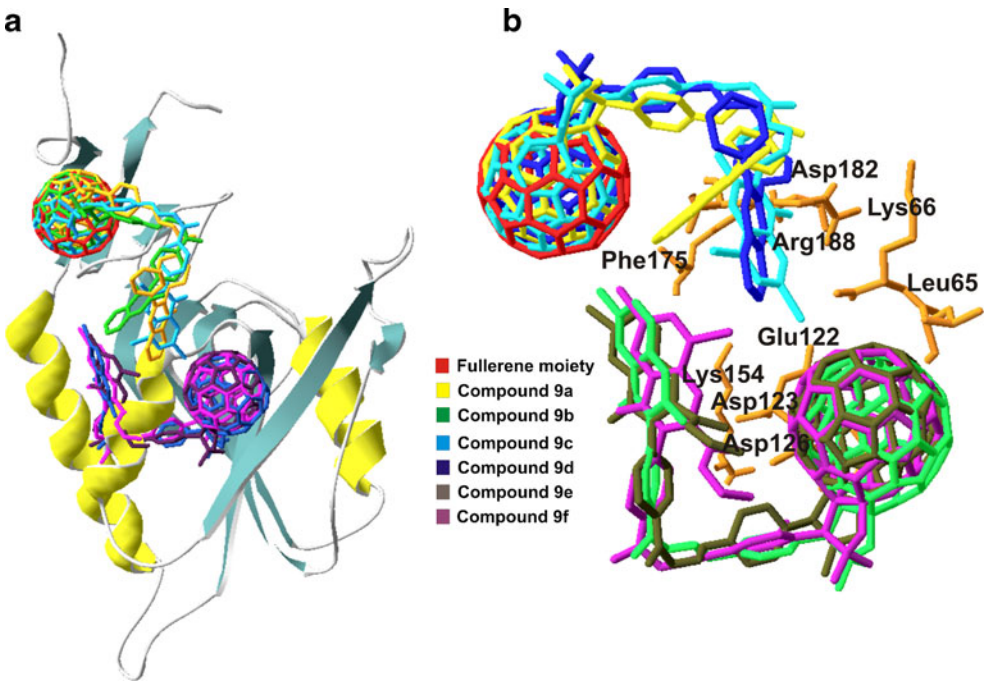

Fig. 6 **a** Docked poses of compounds 9a–f in the M. tuberculosis HGPRT enzyme. **b** A closer view of the molecules' docked poses at the active site

Table 2 Energetic contributions of fullerene and its derivatives **(9a–f)**

Compound	ΔE_{total}[a] (kJ mol^{-1})	H bond term and van der Waals term[a] (kJ mol^{-1})	Electrostatic term[a] (kJ mol^{-1})	Ligand internal energy[a] (kJ mol^{-1})
Fullerene	−49.9251	−48.8825	0.00	−1.0426
9a	−125.8729	−123.5979	−0.6224	−1.6526
9b	−115.2901	−113.4021	−0.1264	−1.7616
9c	−128.9799	−126.6426	−0.6000	−1.7372
9d	−134.6001	−130.0406	−3.1334	−1.4261
9e	−122.9621	−121.2018	−0.2967	−1.4035
9f	−124.6058	−128.2172	−0.1523	−1.2363
	Conformational entropy (kcal mol^{-1})[b]			
9c	8.96			
9f	9.33			

[a]Calculated using iGEMDOCK version 2.1

[b]Estimated using PEARLS (Program for Energetic Analysis of Ligand Receptor Systems) program [48]

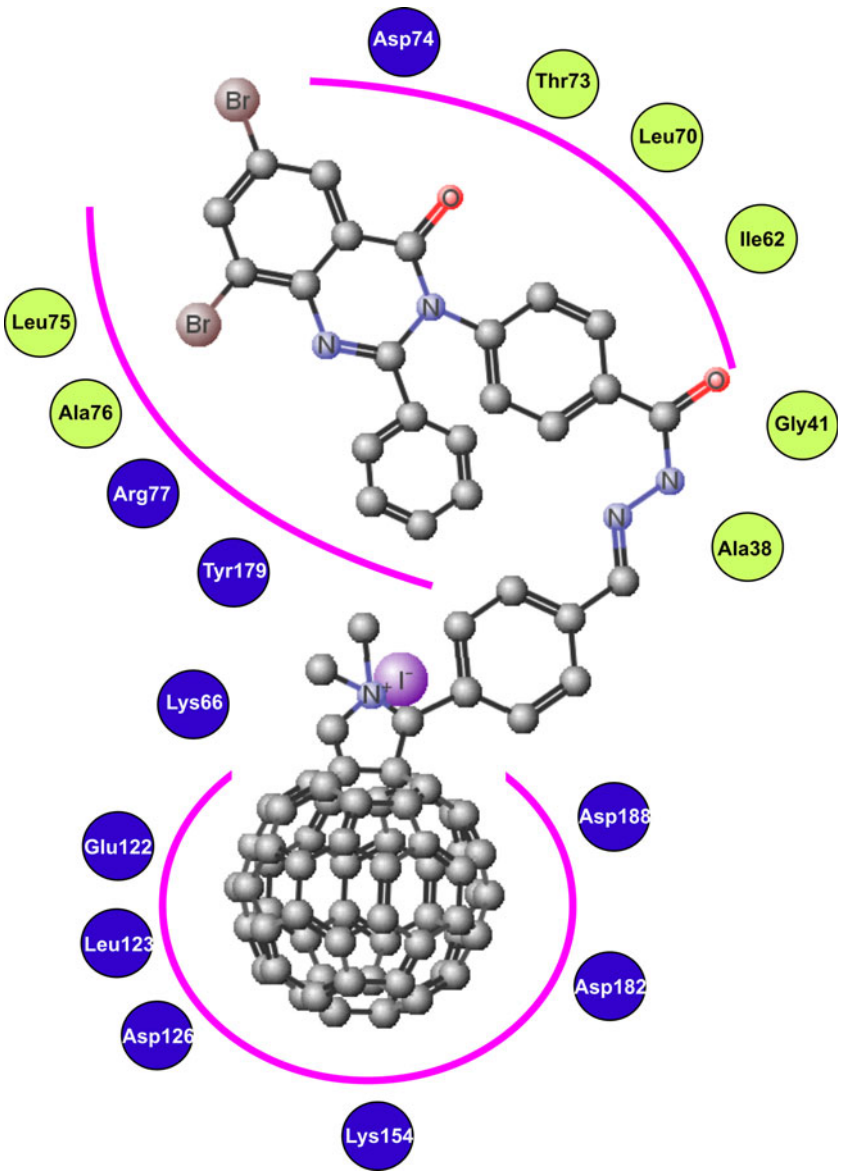

Fig. 7 Two-dimensional representation of compound 9f interacting with key residues of *M. tuberculosis* HGPRT. The H bonding and charged residues are designated by green and blue circles. The receptor surface area exhibiting Π contacts are shown as pink arcs

The compounds in the dataset have a second binding energy in the range of −115.2901 to −134.6001 kJ mol^{-1}, which shows that the molecules interact in a similar fashion. The fullerene moiety of compounds **9a, 9c** and **9d** was found to bind at the first floor, whereas compounds **9b, 9e** and **9f** were observed in the second floor, with all the quinazolinone side arm of the compound set interacting with the common active site loop elements Table 2. Compound **9c** secured a total energy of −128.9799 kJ mol^{-1} with a summed function of H bonding term and van der Waals term of −126.6426 kJ mol^{-1}. Compound **9f** was found to attribute an energetic representation having a total energy of −126.6058 kJ mol^{-1} and summed function of −123.2172 kJ mol^{-1}. The contribution of summed descriptor by compounds **9c** and **9f** was found to be 98.18 % and 98.88 %, which is in good concordance with the fullerene moiety's van der Waals term (97.91 %). In addition, the experimental inhibitory measure, MIC of these compounds (12.5 μg/mL and 3.125 μg/mL) was in good agreement with its computational binding energy predictions.

The following are the amino acids of *M. tuberculosis* HGPRT associated with compound **9f** H bonding: Ala38 (no. of H bonds: 1), Gly41 (1), Ile62 (1), Leu70 (1), Thr73 (2), Asp74 (3), Leu75 (1), Ala76 (1), Arg77 (1) and Tyr179 (1). Hence, it is evident that most of the aliphatic amino acids were preferred by the fullerene side arm to establish H bonding with few charged residues (Asp74, Arg77) (Fig. 7). Owing to the conformational entropy exerted by the molecules with higher activity, compounds **9c** and **9f** were estimated to be 8.96 and 9.33 kcal mol^{-1} using the PEARLS (Program for Energetic Analysis of Ligand Receptor Systems) program [48], respectively. Thus, the binding of fullerene compounds can be summarized briefly in that the conformational entropy required by the fullerene moiety over the floor adjacent to the active site accelerates the proper placement of the aromatic side arm in the cavity, preferably with aromatic amino acids (for instance, Tyr179) and finally constructs a network of H bonds with aliphatic and charged amino acids located proximally.

Conclusions

In conclusion, a novel class of quinazolinone-fullerene conjugates as antimycobacterial agents is reported. Compound **9f** inhibited the growth of *M. tuberculosis* effectively at MIC 1.562 μg/mL, which is in good agreement with the existing front-line drugs, isoniazid (MIC: 0.2 μg/mL) and rifampicin (MIC: 0.25 μg/mL). We conclude that mono- and dibromo-substituted quinazolinone derivatives exhibit better activity than unsubstituted derivatives. Incorporation of bromine atoms into the quinazoline ring increases the lipophilicity of the molecule, allowing it to traverse the mycobacterial cell wall. The contribution of these lipophilic substituents and the positive charges near the fulleropyrrolidine backbone plays an important role in increasing potency. Further, structural analysis of *M. tuberculosis* HGPRT enzyme and its binding mode revealed that the fullerene cage exerts a hydrophobic character and appropriate surface geometry to interact with target whereas the quinazolinone side arm plays a vital role in establishing H bonds with the active site. Our in silico screening approach, accompanied with biological tests, opens a new avenue for the discovery of more efficient anti-tuberculosis drugs. Thus, these molecules constitute important "leads" for further optimization by structure–activity relationship studies to develop effective antimycobacterial agents that can help to shorten the duration of current anti-TB chemotherapy. Further optimization and pharmacokinetic characterization of this series are ongoing in our laboratory.

Acknowledgments M.B.P. thanks the University Grants Commission, New Delhi, India for generous support in the form of a Junior Research Fellowship. S.P.K. and N.N.V. acknowledge generous support from DST, New Delhi in the form of Innovation in Science Pursuit for Inspired Research (INSPIRE) Fellowships.

References

1. WHO (2011–2012) Global facts on tuberculosis. http://www.who.int/tb
2. Butler D (2000) Nature 406:670–672
3. Ahmad SME, Vinsova J, Kratky M, Ngy S, K'ung Z (2010) Nova Science Pub Incorporated 1–328
4. Zhang Y, Young D (1994) J Antimicrob Chemother 34:313–319
5. Kumar SP, Srinivasan P, Patel SK, Jasrai YT, Pandya HA (2011) J Adv Bioinform Appl 2:142–148
6. Kumar A, Menon SK (2009) Eur J Med Chem 44:2178–2183
7. Kumar A, Patel G, Menon SK (2009) Chem Biol Drug Des 73:553–557
8. Dugan LL, Turetsky DM, Du C, Lobner D, Wheeler M, Almli CR, Shen CKF, Luh TY, Choi DW, Lin TS (1997) Proc Natl Acad Sci USA 94:9434–9439
9. Gharbi N, Pressac M, Hadchouel M, Szwarc H, Wilson SR, Moussa F (2005) Nano Lett 5:2578–2585
10. Zhou Z, Lenk RP, Dellinger A, Wilson SR, Sadler R, Kepley CL (2010) Bioconjug Chem 21:1656–1661
11. Kumar A, Rao MV, Menon SK (2009) Tetrahedron Lett 50:6526–6530
12. Zhou C, Liu Q, Xu W, Wang C, Fang X (2011) Chem Commun 47:2982–2984
13. Durdagi S, Supuran CT, Strom TA, Doostdar N, Kumar MK, Barron AR, Mavromoustakos T, Papadopoulos MG (2009) J Chem Inf Model 49:1139–1143
14. Marcorin GL, Da Ros T, Castellano S, Stefancich G, Bonin I, Miertus S, Prato M (2000) Org Lett 2:3955–3958
15. Kumar A, Patel B, Patel G, Menon SK (2010) Fullerenes Nanotubes and Carbon Nanostructures 18:186–197
16. Maeda Mamiya R, Noiri E, Isobe H, Nakanishi W, Okamoto K, Doi K, Sugaya T, Izumi T, Homma T, Nakamura E (2010) Proc Natl Acad Sci USA 107:5339–5344
17. Zakharian TY, Seryshev A, Sitharaman B, Gilbert BE, Knight V, Wilson LJ (2005) J Am Chem Soc 127:12508–12509

18. Foley S, Crowley C, Smaihi M, Bonfils C, Erlanger BF, Seta P, Larroque C (2002) Biochem Biophys Res Commun 294:116–119
19. Lakhan R, Rai BJ (1987) J Chem Eng Data 32:384–386
20. Baba A, Kawamura N, Makino H, Ohta Y, Taketomi S, Sohda T (1996) J Med Chem 39:5176–5182
21. Kumar A, Sharma P, Kumari P, Lal Kalal B (2011) Med Chem Lett 21:4353–4357
22. Kuneš J, Bažant J, Pour M, Waisser K, Šlosárek M, Janota J (2000) Il Farmaco 55:725–729
23. Waisser K, Gregor J, Dostál H, Kuneš J, Kubicová L, Klimešová V, Kaustová J (2001) Il Farmaco 56:803–807
24. Colotta V, Catarzi D, Varano F, Lenzi O, Filacchioni G, Costagli C, Galli A, Ghelardini C, Galeotti N, Gratteri P, Sgrignani J, Deflorian F, Moro S (2006) J Med Chem 49:6015–6026
25. Ducati RG, Basso LA, Santos DS, de Azevedo WF Jr (2010) Bioorg Med Chem 18:4769–4774
26. de Azevedo WF Jr (2011) Curr Med Chem 18:1353–1366
27. Dias R, Timmers LF, Caceres RA, de Azevedo WF Jr (2008) Curr Drug Targets 9:1062–1070
28. Caceres RA, Timmers LF, Ducati RG, da Silva DO, Basso LA, de Azevedo WF Jr, Santos DS (2012) Biochimie 94:155–165
29. de Azevedo WF Jr (2011) Curr Med Chem 18:1255–1257
30. Tang YJ, Ashcroft JM, Chen D, Min G, Kim CH, Murkhejee B, Larabell C, Keasling JD, Chen FF (2007) Nano Lett 7:754–760
31. Freymann DM, Wenck MA, Engel JC, Feng J, Focia PJ, Eakin AE, Craig SP (2000) Chem BioI 7:957–968
32. Gupta SK, Dhawan A, Shanker R (2011) J Biomed Nanotechnol 7:91–92
33. Consortium TU (2012) Nucleic Acids Res 40:D71–D75
34. Altschul SF, Gish W, Miller W, Myers EW, Lipman DJ (1990) J Mol Biol 215:403–410
35. Berman HM, Westbrook J, Feng Z, Gilliland G, Bhat TN, Weissig H, Shindyalov IN, Bourne PE (2000) Nucleic Acids Res 28:235–242
36. Arnold K, Bordoli L, Kopp J, Schwede T (2006) Bioinformatics 22:195–201
37. Ward JJ, Sodhi JS, McGuffin LJ, Buxton BF, Jones DT (2004) J Mol Biol 337:635–645
38. Lindorff Larsen K, Piana S, Palmo K, Maragakis P, Klepeis JL, Dror RO, Shaw DE (2010) Funct Bioinf 78:1950–1958
39. Ramachandran GN, Ramakrishnan C, Sasisekharan V (1963) J Mol Biol 7:95–99
40. Benkert P, Tosatto SCE, Schomburg D (2008) Proteins Struct Funct Bioinf 71:261–277
41. Craig SP, Eakin AE (2000) J Biol Chem 275:20231–20234
42. Chen Q, You D, Liang Y, Su X, Gu X, Luo M, Zheng X (2007) FEBS J 274:4408–4415
43. Gordon JC, Myers JB, Folta T, Shoja V, Heath LS, Onufriev A (2005) Nucleic Acids Res 33:W368–W371
44. Laurie ATR, Jackson RM (2005) Bioinformatics 21:1908–1916
45. Acton A, Banck M, Bréfort J, Cruz M, Curtis D, Hassinen T, Heikkilä V, Hutchison G, Huuskonen J, Jensen J, Liboska R, Rowley C (2000) Chemical 2.00. Department of Chemistry, University of Kuopio, Kuopio, Finland, http://www.uku.fi/~thassine/projects/ghemical/
46. Wolf LK (2009) Chem Eng News Arch 87:48
47. Yang JM, Chen CC (2004) Proteins Struct Funct Bioinf 55:288–304
48. Han LY, Lin HH, Li ZR, Zheng CJ, Cao ZW, Xie B, Chen YZ (2005) J Chem Inf Model 46:445–450
49. Armarego WLF, Chai CLL (2009) Purification of laboratory chemicals. Butterworth-Heinemann, Burlington, MA
50. Maggini M, Scorrano G, Prato M (1993) J Am Chem Soc 115:9798–9799
51. Rather BA, Raj T, Reddy A, Ishar MPS, Sivakumar S, Paneerselvam P (2010) Arch Pharm 343:108–113
52. Alagarsamy V, Muruganantham G, Venkateshaperumal R (2003) Biol Pharm Bull 26:1711–1714
53. Lyon DY, Adams LK, Falkner JC, Alvarez PJ (2006) J Environ Sci Technol 40:4360–4366
54. Anargyros P, Astill DS, Lim IS (1990) J Clin Microbiol 28:1288–1291
55. Scott WRP, Hünenberger PH, Tironi IG, Mark AE, Billeter SR, Fennen J, Torda AE, Huber T, Krüger P, van Gunsteren WF (1999) J Phys Chem A 103:3596–3607
56. Structural Analysis and Verification Server, NIH-MBI Laboratory for Structural Genomics and Proteomics (http://nihserver.mbi.ucla.edu/SAVES/). Structural Analysis and Verification Server, NIH-MBI Laboratory for Structural Genomics and Proteomics (http://nihserver.mbi.ucla.edu/SAVES/)
57. Pearlman DA, Case DA, Caldwell JW, Ross WS, Cheatham TE III, DeBolt S, Ferguson D, Seibel G, Kollman P (1995) Comput Phys Commun 91:1–41
58. Wang J, Wolf RM, Caldwell JW, Kollman PA, Case DA (2004) Comput Phys Commun 25:1157–1174